Epitope Fluctuations in the Human Papillomavirus Are Under Dynamic Allosteric Control: A Computational Evaluation of a New Vaccine Design Strategy
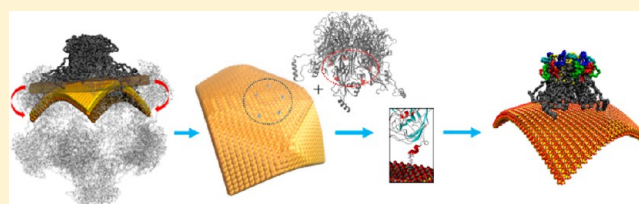
Abhishek Singharoy,[†,§] Abhigna Polavarapu,[†,§] Harshad Joshi,[†] Mu-Hyun Baik,*[,†,‡] and Peter Ortoleva*[,†]

[†]Department of Chemistry, Indiana University, Bloomington, Indiana 47405, United States
[‡]Department of Materials Chemistry, Korea University, Jochiwon-eup, Sejong-si, 339-700, South Korea

S Supporting Information

ABSTRACT: The dynamic properties of the capsid of the human papillomavirus (HPV) type 16 were examined using classical molecular dynamics simulations. By systematically comparing the structural fluctuations of the capsid protein, a strong dynamic allosteric connection between the epitope containing loops and the h4 helix located more than 50 Å away is identified, which was not recognized thus far. Computer simulations show that restricting the structural fluctuations of the h4 helix is key to rigidifying the epitopes, which is thought to be required for eliciting a proper immune response. The allostery identified in the components of the HPV is nonclassical because the mean structure of the epitope carrying loops remains unchanged, but as a result of allosteric effect the structural fluctuations are altered significantly, which in turn changes the biochemical reactivity profile of the epitopes. Exploiting this novel insight, a new vaccine design strategy is proposed wherein a relatively small virus capsid fragment is deposited on a silica nanoparticle in such a way that the fluctuations of the h4 helix are suppressed. The structural and dynamic properties of the epitope carrying loops on this hybrid nanoparticle match the characteristics of epitopes found on the full virus-like particle precisely, suggesting that these nanoparticles may serve as potent, cost-effective, and safe alternatives to traditionally developed vaccines. The structural and dynamic properties of the hybrid nanoparticle are examined in detail to establish the general concepts of the proposed new design.

INTRODUCTION

Virus-like particles (VLPs) are assemblies of multiple proteins that mimic the organizational features of viruses including repetitive surface particulate structures such that they may elicit a pathogen-associated molecular pattern recognition response by the innate immune system.[1−7] Because they are devoid of genetic material, VLPs provide a safer and more cost-effective alternative to traditional vaccine development methods, and several high-priority viruses[1] have been targeted, namely the human papillomavirus (HPV)[8−10] (Gardasil[11,12] and Cervarix[13,14]), Chikungunya,[15,16] and hepatitis E[17,18] viruses. Despite these promising developments, the impact of VLPs on vaccine design at large remains limited, in part because many technical and fundamental challenges are currently unsolved.[1,7,19−25] For example, Gardasil is a very successful VLP-based vaccine that comprises of a mixture of VLPs derived from the L1 major capsid proteins of four different HPV types, namely 6, 11, 16, and 18. Gardasil induces specific antibody responses against these HPV types.[26−29] However, with more than 40 oncogenic HPV types identified to date,[30,31] it is clear that the capabilities of current vaccine design technology must be expanded to enable a broader spectrum of protection. Traditional vaccine design approaches rely on cost-intensive, repetitive laboratory procedures and testing protocols. As a result, vaccine development is a time-consuming and costly undertaking.

One possible way of streamlining the discovery process is to utilize computer-aided design strategies to narrow the search and better understand the properties of various VLPs. By exploring the structural and dynamic features of a VLP *in silico* and correlating them to experimentally observable efficacy data, the most salient molecular features of the VLP that may give rise to the immunogenicity can be identified. Exploiting these properties will enable a rational design approach that may significantly shorten vaccine development time. Due to their enormous size, probing the dynamic structure of a VLP under realistic conditions requires computationally intensive molecular dynamics (MD) simulations. The advent of high-performance computing platforms[32−34] and sophisticated modeling algorithms[35,36] made these daunting simulations within reach.[37−39]

Here, we extend our previously adopted strategy of applying MD simulations for the *in silico* construction and molecular level analysis of candidates for VLP vaccines.[36,40] Specifically, HPV type 16 is examined, as (i) an all-atom X-ray structure with known epitope regions is readily available[41−43] and (ii) well-defined molecular level properties thought to be responsible for the immunogenicity were previously identi-

fied.[44−47] These VLPs can be assembled either from 12 or 72 pentamers of the L1 protein arranged in a $T = 1$ or 7 icosahedron structures, respectively.[42,43,47] Whereas Gardasil is based on $T = 7$ L1 icosahedral structure, Cervarix is an alternative HPV vaccine that is based on a $T = 1$ L1 structure. The assemblies are stabilized by strong hydrophobic interactions.[41,43] The C-terminus of the L1 protein consists of four helical regions h2, h3, h4, and h5 that are responsible for intra- and intermolecular stabilization, as illustrated in Figure 1a. The domains h2, h3, and h5 are responsible for maintaining
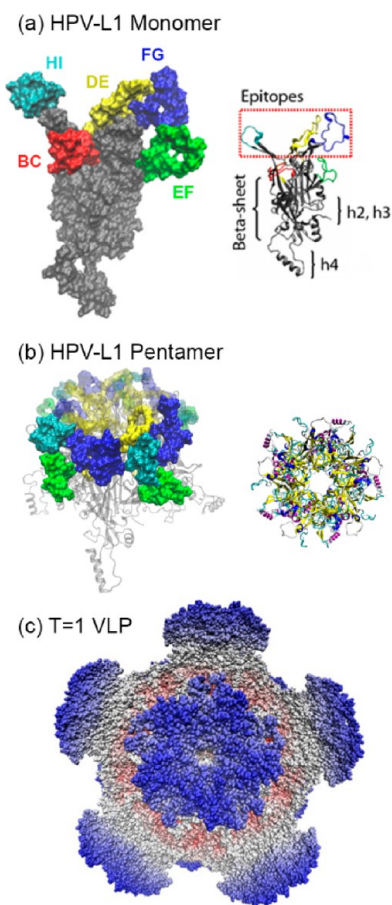

Figure 1. The structures the VLP components: (a) The isolated HPV-L1 monomer. The protein is depicted in gray with five different epitopes presented in red (BC), yellow (DE), green (EF), blue (FG), and cyan (HI). (b) HPV-L1 pentamer (c) HPV particle consisting of 12 pentamers arranged in $T = 1$ icosahedral structure.

the structural integrity of the pentamer, and h4 preserves the interpentamer connectivity, thereby determining the overall structure. The VLP surface has outwardly projecting protein loops containing epitopes that interact with the immune system to elicit production of type-specific antibodies.[48] Antibodies binding to the epitopes often render the associated virus/VLP inactive and neutralized. Neutralization assays of HPV-16 VLPs with human sera were used to identify five epitope bearing loop regions denoted BC (residue 49−70), DE (110−154), EF (170−189), FG (262−291) and HI (347−360).[41,43,49] These loops are thought to be more flexible than the rest of the L1 monomer and show notable conformational differences across HPV types.[48] Epitope deletion strongly affects the antibody-binding capacity of the VLPs[44] and reduces their immunogenicity by a factor of at least 10−20 compared to wild-type

VLPs.[50] There are several characteristics of VLP epitopes that may influence specific immune response; these properties include peptide sequence, loop conformation, and proximity/orientation relative to neighboring loops.[41,43]

The exact molecular-scale relationship between epitope structure and immune response is difficult to establish. For example, if individual epitope characteristics such as shape or sequence were the only factors relevant for immunogenicity, an L1 protein monomer or L1 pentamer could serve as a vaccine. However, the monomer is essentially not at all immunogenic, and the pentamer is only weakly so,[51] in contrast to the highly immunogenic whole VLP. This difference in immunogenicity cannot be explained by the assumption that a VLP contains more epitopes than a pentamer or a monomer; as the increase in the monomer/pentamer dosage (and hence the number of epitopes) does not imply any associated increase in the HPV immunogenicity.[51] The epitope geometry among these structures is also very similar.[49] Furthermore, weakly organized VLP assemblies are found to be less immunogenic than more tightly packed ones.[52] One explanation of these observations comes from the fluctuation-immunogenicity hypothesis: To illicit proper immune response, epitope fluctuations must be minimized,[40] such that the epitope structures are better defined and rigid over time; in tightly packed VLPs the epitope fluctuations are less pronounced than those in smaller systems. In other words, simply presenting an epitope to the immune system is not enough, as the structural fluctuations may render them unrecognizable. This hypothesis emphasizes the importance of understanding the dynamics of epitope structure and suggests that the immune response to the smaller, simpler assemblies could be improved if the structural fluctuations can be reduced. Allosteric effects are widely recognized as central to controlling structure and dynamics of high-order protein assemblies,[53−68] and the tightly packed VLP constitutes a highly illustrative example of such long-range control. In particular, we found that epitope structure and function are strongly affected by allosteric interactions with the h4 helix of the L1 protein. We envisioned that this key interaction may be reproduced by tethering the L1 protein to a silica surface, thus mimicking the structure and conformational dynamics of the epitopes in the much more complex VLP assembly using a bioinorganic hybrid construct consisting of a silica nanoparticle and a much smaller piece of the virus. In this design the L1 protein is tethered to silica surfaces covalently. We examined how the epitope structure and dynamics are modulated by changing the curvature of the silica particle model and surface protein concentration. Interestingly, we found that the proposed bioinorganic mimics have epitope properties of the wild-type VLP but do so in a way that (i) does not require construction of large T-numbered assemblies, (ii) facilitates easy synthesis, and (iii) are genome-free and more stable than a pure macromolecular assembly. A similar construct was previously considered experimentally in the context of designing a vaccine against Porcine Circovirus Type 2[69] and is already in trials.[70] Here, we extend such ideas to HPV 16 VLP vaccines and quantitatively assess the role of the silica nanoparticle on the structure and, importantly, the dynamics of the epitopes attached to it.

■ METHODS AND MATERIALS

Model Preparation. The models presented in this work include L1 monomer, pentamer and $T = 1$ VLP in various arrangements and on different silica surface geometries connected via covalent tethers.

All-atom, explicit solvent MD simulations were performed using NAMD[71,72] 2.7 for 10 ns on each of these assemblies. Atomic coordinates of the L1 monomer are obtained from the crystal structure (PDB code: 1DZL).[42] To validate the allosteric effect of the h4 helix (residue 414−434), test simulations were performed on h4 helices that were truncated and artificially rigidified. The $T = 1$ VLP is constructed from 60 copies of the monomer using icosahedral symmetry transformations (from VIPERDB).[73] The pentamer is extracted from this VLP to maintain structural continuity with the latter. All systems considered are immersed in a box of TIP3P waters,[74] extending at least 20 Å from the surface of the protein models. A 0.3 M NaCl buffer solution was introduced to mimic the conditions under which the experiments we conducted, using the VMD[75] auto ionize feature. The resulting solvated system sizes range from $\sim 10^5$ to $\sim 10^6$ atoms. The 20 × 20 nm silica surface is generated by creating the appropriate images of the central unit cell using the IMAGE facility in CHARMM.[76,77] The silica model has a thickness of 5 nm incorporating 2 core layers of tetrahedral silicate moieties and surface layers including hydrophilic (Si−OH) and hydrophobic (Si−H) groups on opposite ends. Curvature is introduced in the silica surface via steered MD simulations. The silica surface is functionalized with aliphatic-amino tethers that can covalently hold the L1 protein to the silica surface, and have simple electronic properties. CHARMM27[78] force fields are used for protein simulations. For simulating the silica surface, force fields developed by MacKerell were used.[79] For the simulations where the protein was attached to the silica surface with the tether, the parameters for silicon atoms were slightly modified so that all the force fields were compatible to each other. A systematic procedure using high-level quantum calculations[80] were employed to develop the force fields for the tether molecule, as detailed in the Supporting Information.[81,82]

MD Simulation Details and Associated Analysis. All MD simulations were run on PowerPC 970MP processors of the BigRed supercomputer at Indiana University. Details of simulation settings are provided in the Supporting Information. To distinguish the behavior of the simulated constructs in terms of loop structures and their fluctuations, following molecular scale measures were considered. Here, we focus on the analysis of the FG loop (residue 262−291) as it is found to be most relevant for eliciting immune response; for certain comparison, the EF and HI loops are also considered.[49] Similar results hold for the other epitopes.

Dihedral Distribution for Loops. The distribution of backbone loop dihedral angles is a good indicator for the conformational space explored by the epitope containing loops and provides a measure of the flexibility of the loop. In each case, 10 000 time points were extracted from MD simulations to construct the probability distribution of loop conformations. Since distribution from a randomly selected half of the ensemble is found to accurately reproduce the other half, analyzed structures are representative of the phenomenon of interest.

Power Spectra. The power spectrum provides the distribution of atomic vibration intensity across a range of frequencies. Lower frequencies represent slower motions, while high frequencies represent faster modes. These measures were used to discriminate between the energies of different frequency motions of a given loop type as manifested in an assembly of a given size (i.e., from L1 monomer to $T = 1$ VLP). Simulations were designed to assess potential differences in behavior of loops between the L1 protein assemblies and quantify them to serve as a basis of our computer-aided vaccine discovery strategy. This study focused on loops known to contain critical epitopes, some of which are neutralizing.

Positional Variance. The overall fluctuations of a particular loop from its average configuration were compared. Loop fluctuation is not easily quantified in X-ray or cryo-EM data. While a structure provides the most likely or average configuration, its fluctuation measures the importance of other configurations away from the average, but which may be functionally relevant within the framework of our immunogenicity hypothesis. Information about the dynamics obtained from MD provides advantages over the inherently averaged experimental data. Positional variance of the loop atoms was quantified

as another measure of epitope fluctuation. Positional variance was computed by summing over the deviation of individual backbone atom position and dividing by the number of backbone atoms in the loop. This measure is slightly different from the usual root-mean-square fluctuation (RMSF). RMSF measures fluctuation from a fixed reference structure by aligning two structures, thus eliminating translational and rotational motions. In contrast, average loop positional variance calculated here contains contributions from overall displacements of the loops and their motions relative to the rotation/translation and internal motions of the assembly. The overall motions potentially affect epitope location and orientation within loops; according to our hypothesis, these overall fluctuations also affect immunogenicity and binding properties of the monomer or larger assemblies. Thus, including the effect of overall and internal assembly motions on loop fluctuations provides a more complete measure of their potential relevance to immunogenicity.

Energy Analysis, Contact Maps, and Hydrogen Bonds. We also performed energy, contact map, and hydrogen bond analyses. They were carried out on each trajectory using standard tools available in VMD.[75] In particular, energies were computed using the NAMD Energy plugin. Contact between two residues is considered if they were within a cutoff of 10 Å and neglected if the inter-residue distance exceeds the cutoff. Finally, hydrogen bonds were defined solely on the basis of geometric parameters (bond angle: 20°; bond length: 3.8 Å) between donors and acceptors. Analysis of interplay between these properties for each of the simulated constructs yielded insights into interactions between the pentamer, tether, and silica surface.

Correlation Analysis. The pairwise correlations measuring the standard inter-residue three-dimensional orientational coupling were computed using the covariance between positions of the ith Cα atom at time t with respect to its initial value along the computed trajectory. A time averaged covariance matrix was built as

$$\langle C_{ij} \rangle = \frac{1}{T} \int_1^T \Delta \hat{r}_i(t) \cdot \Delta \hat{r}_j(t) \, dt$$

where $\Delta \hat{r}_l$ is the unit vector of the displacement of the ith C$_\alpha$ atom at time t, and T is the length of time over which we calculated the covariations. Positive correlations indicate correlated motion between the two residues, whereas negative values correspond to anticorrelation. Correlations with magnitude <0.5 were considered statistically insignificant and therefore neglected.

RESULTS AND DISCUSSIONS

Dynamic Properties and Structural Fluctuations. Figure 1a shows a space filling model and a cartoon representation of the HPV-L1 protein monomer. The epitope bearing loop regions denoted BC (residue 49−70), DE (110−154), EF (170−189), FG (262−291), and HI (347−360)[41,43,49] are marked in red, yellow, green, blue, and cyan, respectively. Five monomers assemble into a HPV-L1 pentamer, as illustrated in Figure 1b, and 12 pentamers can finally be arranged in a $T = 1$ icosahedral structure to afford the VLP, shown in Figure 1c. Of the five loops the FG loop is most important for eliciting immune response, followed by the EF and HI.[49] The BC and DE loops are thought to be less important. Therefore, we concentrate on the FG, EF, and HI loops[83] in this work.[49] To examine the structural fluctuations and dynamic properties of the epitopes in this series of increasing complexity, we calculated the backbone dihedral angle distributions, positional variance, and power spectra at each stages of assembly. Not surprisingly, the dihedral angles show the narrowest range in the VLP followed by the pentameric structure and display the widest range in the monomeric form (Figure S3a), which is simply an indication of the increasing compactness as we move from the monomer to the VLP. Similarly, the positional variance of the loop fluctuations is largest in the monomer with amino acid
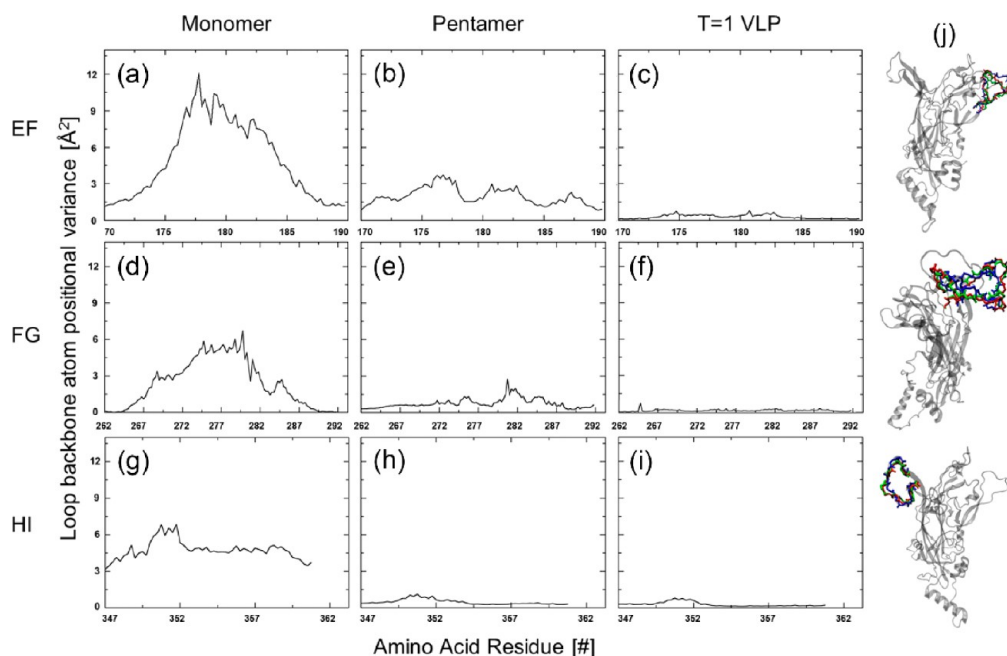
Figure 2. Backbone atom positional variance for L1 monomer (left), pentamer (middle) and $T = 1$ VLP (center). For each loop X-axis denotes the residue number and Y-axis denotes fluctuation in Å^2. Like the spread of the dihedral distributions (Figure SI3), the positional variance decreases as assembly size increases. The fourth column shows mean orientation of the epitopes suggesting they change minimally between the monomer (blue), pentamer (red), and VLP (green).

positions showing variances as large as 12 Å^2 in EF and 7 Å^2 in FG and HI loops, as shown in Figure 2a,d,g. In the pentamer these positional variances decrease significantly with the maximum not exceeding 3.5 Å^2 in all cases (Figure 2b,e,f). Finally, the fluctuations in the amino acid positions become negligible in the $T = 1$ VLP, as illustrated in Figure 2c,f,i. The high-resolution profiles summarized in Figure 2 illustrate that the loops are rigidified substantially as the monomers are assembled into the pentamer. Although further stiffening occurs when the pentamers are combined to give the final VLP, the change in positional variance is much less pronounced, supporting the idea that the full-scale VLP may not be necessary to mimic the epitope dynamics sufficiently. As expected, the power spectra show a successive decrease in the low-frequency region upon forming the pentamer and the VLP. At higher frequency, the power spectra for the three constructs are similar because short time scale motions like bond oscillations are similar for all three assemblies (Figure S3c). These results establish a consistent trend of decreasing structural flexibility of the epitopes as the assembly process progresses from monomers to the full VLP; the dynamic behavior of an epitope is therefore heavily influenced by the neighboring regions of same protein and the presence of other proteins. Interestingly, the mean structure of the epitopes remains practically identical in all constructs, as shown in Figure 2j, where the mean structures of EF, FG, and HI loops in the monomeric, pentameric, and VLP constructs are compared by overlaying them. This conclusion is somewhat unexpected, as it is intuitively plausible that the organization of the epitope carrying protein into the higher order constructs should impact both the structure and dynamics of the protein. The fact that the mean structure of the epitope in smaller constructs is identical to that of the whole VLP is critically important, however, as this structural fidelity is a necessary, but not sufficient, requirement for utilizing smaller virus fragments

to elicit the antiviral immune response. This result is particularly interesting within the context of the aforementioned experimental observation that the monomeric protein and the pentamer are essentially not immunogenic[51] and suggests that this failure is due to the dynamic flexibility of the epitope in these constructs. To make the simpler constructs immunogenic, we must better understand the origin of the structural fluctuations and find means of inhibiting the positional variance in them.

One important factor for decreasing epitope fluctuations is structural confinement and inertial effects of the L1 assembly as its size increases.[51] A monomer has the lowest weight, and the epitopes are least confined; therefore, associated fluctuations are maximum. In the pentamer and subsequently the VLP, both epitope confinement and assembly inertia increase notably, suggesting a significant decrease in structural fluctuations. For example, HI from one monomer is confined by FG from its counterclockwise neighbor (Figure 1b). Similarly, FG interacts with loops DE and HI from its clockwise neighbor. This structural confinement from interepitope interactions is particularly effective for loop HI, as shown in the positional variance diagrams Figure 2g → 2h → 2i. On the other hand, loop EF lacks interepitope contacts and is more solvent accessible than FG or HI. Thus, it preserves some of its structural fluctuations in the pentamer, as illustrated in Figure 2a → 2b and becomes fully confined in the VLP (Figure 2c). In other words, the neighboring proteins inhibit structural fluctuations of the epitope carrying loops simply by occupying the space that is needed to execute some of the structural fluctuations. Second, epitopes are subjected to identical increase in inertia as the system size increases, which will dampen structural fluctuations of all epitopes. Thus, confinement and increased inertia give a plausible overall trend, but specific interepitope interactions are important and must be examined
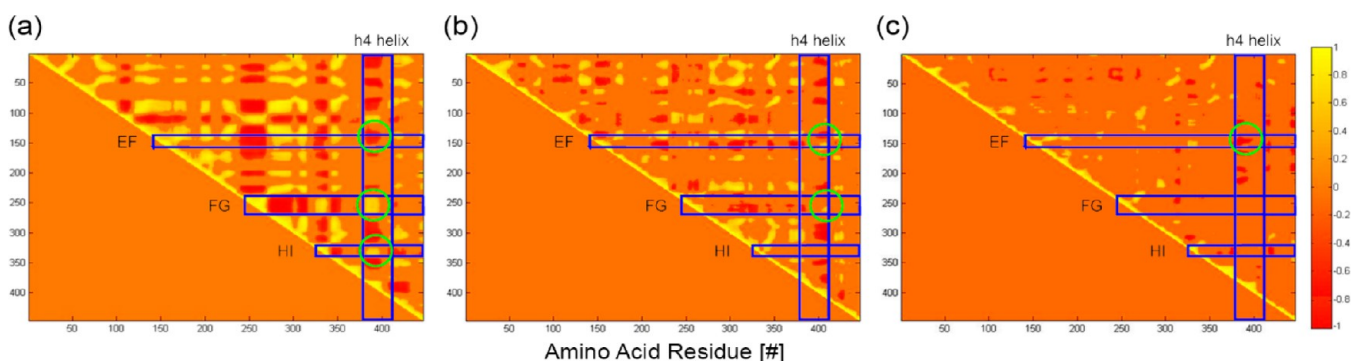
Figure 3. Covariance matrices from 10 ns trajectory of (a) an isolated L1 protein, (b) an isolated pentamer, and (c) $T = 1$ VLP.

in greater detail to understand the nonuniform changes in fluctuations.

The tertiary structure of an L1 monomer is composed of β-sheets that carry the epitopes and α-helices on either end, as illustrated in Figure 1a. To better understand how these different components interact with each other and modulate the fluctuations, we constructed a covariance matrix from a 10 ns trajectory, shown in Figure 3a. In this diagram, strongly correlated structural distortions can be identified by high correlation coefficients that are marked by bright yellow and bright red spots in the diagram. Correlation coefficients smaller than |0.5| can be considered statistically independent. Not surprisingly, all epitope carrying loops show significant correlation, as they are spatially close and structural distortions of one loop will cause steric clashes with another loop. Surprisingly, strong correlations are seen between the highly flexible h4 helix and all epitopes with correlation coefficients that are consistently larger than |0.6|, marked in green in Figure 3a for the three loops of interest in this study. This strong communication is unexpected, as h4 is on the opposite side of the protein and the distance between the center of the h4 helix and the center of the FG-loop, for example, is 55.3 Å. It is not obvious how structural fluctuations in the helix will be mediated by the epitope region of the protein over such a long distance. To further investigate this unusual coupling, we designed a computational experiment by manually changing the force fields associated with the amino acids in the h4 helix,[84] as to artificially rigidify the helix and simply freeze the h4 helix structurally. If the fluctuations of the h4 helix and those of the epitope loops are truly coupled in an allosteric fashion, this artificially induced rigidity on the h4 helix should be translated to the loops, and our simulations should show a reduced positional variance for the loops. The positional variance plot for the FG loop is given in Figure 4 and illustrates that loss of structural fluctuations in the h4 helix are indeed reported to the FG loop. The positional variance of the residues 267−280 that are part of the FG-loop is greatly reduced from 3 to 7 Å^2 in the original protein (black line in Figure 4) to 1−3 Å^2 (orange line in Figure 4); similar observation can also be made for the other loop regions. Thus, allosteric interactions between the h4 helix and epitopes play a major role in modulating epitope fluctuations. Whereas all epitopes show dynamic allosteric coupling to the h4 helix in the monomer, as indicated by the high correlation coefficients shown in Figure 3,[85] the variation of this coupling with the assembly into higher order constructs is notably different from each other. In the monomer, the differences in fluctuation between epitopes mostly arise from intramolecular confinement. For instance, since FG is more
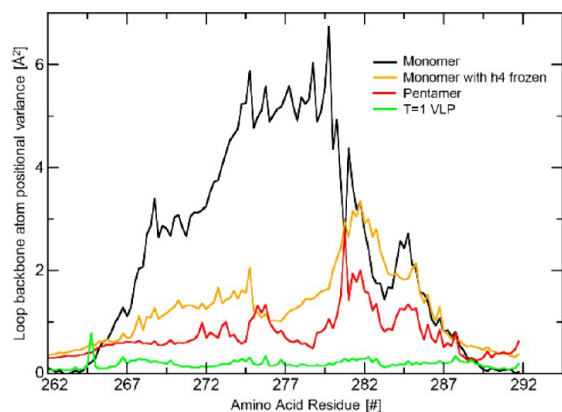

Figure 4. Positional variance for the FG loop fluctuations of free L1 protein, L1 protein with the h4-helix artificially frozen, pentamer, and $T = 1$ VLP.

confined than HI its fluctuations are dampened: Almost all of the amino acids in the HI-loop can engage in fluctuations giving rise to the positional variances of the backbone atoms of these residues to be higher than 4 Å^2 consistently, with the maximum variance being around 7 Å^2 (Figure 2g). Amino acids in the FG loop display a distinctively different variance profile. Whereas the maximum variance is comparable at ∼6 Å^2 (Figure 2d), there are many amino acids that show only small positional variances affording a profile that covers a range of 0−6 Å^2, unlike in the HI loop where the range was 3−7 Å^2. When multiple L1 proteins are brought together, the epitopes arrange on the surface, and the h4 helices are either solvent exposed in the pentamer or they penetrate neighboring pentamers via hydrophobic interactions which stabilize the VLP core. In the higher order assemblies, additional confinement and strong intermolecular interactions decrease epitope fluctuation compared to the free monomer, simplifying the covariance matrices significantly, as shown in Figure 3b,c. Most interestingly, the FG and EF loops remain correlated to the h4 helix in the pentamer, as highlighted in green on Figures 3b. The positional variance of the amino acids in the pentamer, shown in red in Figure 4, shows a striking similarity to the profile we obtained by simply freezing the h4 helix (orange in Figure 4). Both the magnitude and shape of the variance profiles are very comparable, suggesting that the main reason for diminished fluctuation of the FG loop in the pentamer is the change in chemical environment of the h4 helix, which leads to an allosteric stiffening of the epitope containing loops. In the VLP, only the EF loop maintains a correlation to the h4 helix (Figure 3c), but this finding must be interpreted with caution, as the

loops in the VLP are practically rigid structures showing little to no structural variation. Whether or not these small positional variances are correlated to the h4 helix bears little chemical meaning. Interestingly, the allostery does not invoke any significant changes in the mean structures of the epitopes. Instead, the allosteric connection is expressed in variations of structural fluctuations, which in turn impact the biochemical behavior of the epitopes.[86]

This finding is interesting from a general perspective about allosteric interactions in proteins. Traditionally,[53−55,57,62,87−89] allosteric interactions involve a small molecule binding event at one site of a protein that triggers a structural change at a different site, which is accompanied by reactivity changes at that site. Recently, this classical view of allosteric interactions has been extended, and there is growing awareness of the fact that the modulation of chemical behavior does not have to be related to structural changes necessarily.[56,58,59,61−63,90−92] Changes in the entropy profile of molecular fragments can be just as powerful in modulating the chemical behavior[56,93,94] giving rise to dynamic allosteric effects,[95] the most prominent manifestation of which is the change in structural fluctuation; this type of allosteric control may be referred to as "nonclassical allostery", as to emphasize the distinctively different underlying mechanism of remote controlling the chemical property. Our study goes one step further in generalizing the concept of dynamic allostery in that we find that the dynamic coupling between two strongly correlated sites is general and substrate binding is only one of many possible ways of changing the chemical properties of a molecular fragment. In this case, the mean structure of the epitope containing loops remains practically invariant across the sequence of L1 constructs noted above, but the function and biochemical reactivity of these loops are nonetheless altered significantly, as the structural flexibility of the epitopes are modified. Our current work constitutes a rare demonstration of a strong dynamic allosteric effect across a long distance of 55 Å, where the allosteric signal transduction pathway contains standard peptidyl building block. In a previous theoretical study,[96] long distance dynamic allostery was envisioned to require structurally rigid components. Our findings suggest that these long-range correlations may be more common than thus far envisioned and that they do not require specially constructed, exotic entities to establish the dynamic allostery.

Rapid and large structural fluctuations of the epitopes are expected to reduce the antibody binding affinity[40] and diminish the immune response. Depending upon micro-environmental conditions the population of the L1 assemblies will shift from one form to another, e.g., analytical ultracentrifugation and light scattering analyses show that at a pH of ~6 and salinity >0.5 M NaCl a $T = 1$ or $T = 7$ VLP structure is stable; at pH 8.2 they dissociate into L1 sub assemblies.[52] Larger assemblies exhibit lower levels of epitope fluctuation that facilitates stronger affinity for antibody binding.[40,51] However, some epitope fluctuation is required to allow antibody binding due to entropic enhancement of the epitope-antibody binding free energy.[97] Thus, there is an optimal level of epitope fluctuation intensity at which binding is favored, and beyond which the entropic barrier to binding becomes significant. Simulations suggest that the optimal fluctuation level is at <1 Å/residue, which is observed in the VLP illustrated in Figures 2c,f,i. Finally, the allosteric scheme presented here is positively co-operative, i.e., the association of the h4 helices within the pentamer gives rise to an optimal epitope fluctuation level that,

in turn, promotes antibody binding and subsequent immune response. A more quantitative and detailed study of the energetics involving the allosteric signal transduction pathway and epitope-antibody binding is required to decipher the exact mechanism of our suggested allostery. This is beyond the scope of the present study and is partly addressed elsewhere.[98] In this work, we questioned how the insight discussed above can be exploited, and we considered a strategy for silica-based hybrid nanoconstructs where HPV substructures are attached to a silica nanoparticle in a way that will mimic the epitope properties of an entire $T = 1$ VLP.

Hybrid Nanoparticles. Given the strong allosteric correlation between the epitope containing loops and the h4 helix examined above, one potentially effective way of controlling the dynamic properties of the loop regions is to modify the chemical environment of the h4 helix. To allow fluctuation of L1 epitopes in the sub Å range, which corresponds to the fluctuations seen in the $T = 1$ VLP and which we assume to be the optimal range of fluctuations for eliciting immune response, we first attached the L1 protein to a model silica surface only using the innate electrostatic and hydrogen-bond-based attraction between the h4 helix and the silica surface. After some experimentation, we chose to present the hydrophilic 100 surface of crystalline silica, where each terminal surface oxygen of the silicate was protonated, to the h4 helix of a single L1 protein. The model surface was 20 × 20 nm large and had a thickness of 5 nm incorporating 2 core layers of tetrahedral SiO_2 moieties. This design is shown in Figure 5a, where only a
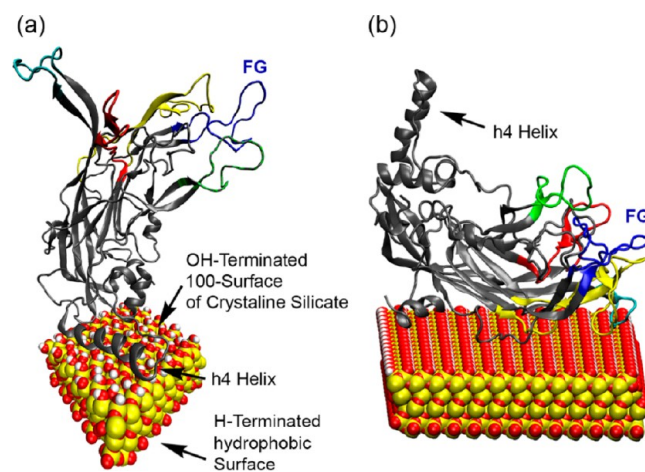

Figure 5. Proof-of-principle models of silica-bound L1 proteins where (a) the h4 helix and (b) the β-sheet portions are connected to the silica surface.

small portion of the 400 nm² silica surface is shown for illustration. The surface layers were properly terminated with hydrophilic (Si−OH) and hydrophobic (Si−H) groups on each side of the silica sheet. Due to the finite size of the silica sheet chosen to make the simulations computationally feasible, buckling is observed in the silica-water simulations. To avoid such buckling of the surface, harmonic restraints are used on the hydrophobic silica layer that is furthest from the L1-binding surface. However, the surface in contact with the protein is kept unconstrained so that surface fluctuations can affect protein dynamics. This is a reasonable approximation that is commonly used in studies involving silica sheets.[99] The positional variance that results from letting the h4 helix interact with the silica surface is shown in Figure 6 in cyan color. As seen above, all
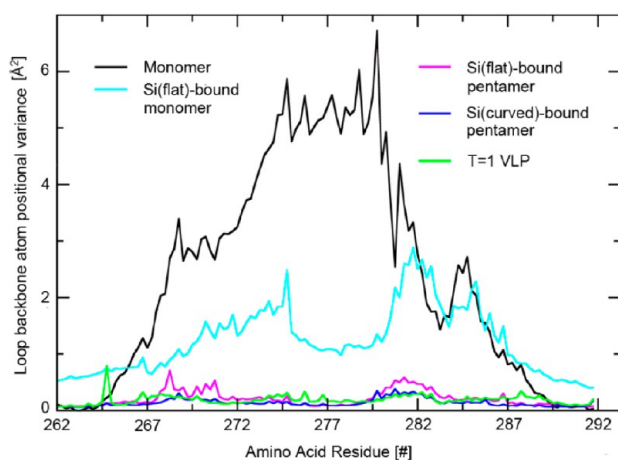
Figure 6. The positional variance profiles of the silica-bound protein constructs. The profiles of the monomer and $T = 1$ VLP are shown as references.

epitope fluctuations decrease significantly, and the variance of almost all amino acids in the FG-loop is <2 Å^2. The extent of fluctuation dampening and the shape of the positional variance profile is remarkably similar to what we found when we artificially inhibited the h4 fluctuations (Figure 4, orange line), indicating that our basic design idea is plausible and that restriction of fluctuations of the h4 helix is faithfully coupled to the FG loop leading to diminished loop fluctuations.

Whereas the model above is encouraging, it is not probable that the L1 monomer will self-assemble into the desired structure where only the h4 helix has contact to the silica surface, while the rest of the L1 protein maintains its overall structure. In fact, we found that a different structure, where the β-sheet portion of the L1 protein gains contact with the surface, is energetically more preferable in good agreement with the notion that β-sheets can bind strongly to silica surfaces.[100] Among the many possible adducts, one is shown in Figure 5b. The contact between the β-sheet and the silica surface is maximized, and the h4 helix points away from the surface and, thus, none of the conceptual design motif initially envisioned is incorporated in this energetically more feasible structure. From a possible vaccine design perspective this protein-silica association is undesirable, as the structure of the protein as a whole and the mean structures of the epitope carrying loops are compromised significantly. As these latter structures are energetically favorable and intuitively plausible, it is safe to conclude that a self-assembly approach to preparing the desired L1-silica hybrid system is not promising to succeed. In addition, all of our monomer simulations suggest that the cooperative confinement that is present in the pentamer is needed to further reduce the positional variance to the desirable range of <1 Å^2.

A more complex design that may offer a solution to the problems identified above and provide a more realistic bioinorganic nanoparticle is to place the L1 pentamer on the silica surface and control the protein-silica contact points by using covalent linkages. Several strategies are readily available for attaching proteins to a solid support.[101] For example, the silica surface can be treated with amino silanes to afford a uniform surface layer of primary amines,[102,103] which we modeled using terminal $-Si-O-(CH_2)_3-NH_2$ moieties on the silica surface. The L1 proteins can be covalently linked to such an activated surface by a peptide coupling reaction[104] to afford

a permanent amide tether[102] containing a silica$-Si-O-$ $(CH_2)_3-NH-CO-L1$ motif, where the tether is anchored at the h4 helix. This design overcomes shortcomings of the monomer-silica structure as (i) interactions between epitopes that are located on different L1 proteins in the pentamer are maintained, (ii) the covalent linkage provides control over the silica-protein contact point and suppresses structural degradation that may arise from undesirable interactions between the β−sheet portion of L1 and the silica surface, and (iii) the h4 helix fluctuations will be inhibited both by the covalent linkage and noncovalent interactions of the h4 helix with the silica surface, as demonstrated in our small model above. Use of silica with aliphatic-amino tethers in the construction of hybrid VLPs has several attractive features: silica has a highly tunable surface chemistry which facilitates conjugation with biological entities,[105] is essentially transparent to light,[106] and is nontoxic and biocompatible.[107] However, like most other nanomaterials, including gold or magnetic nanoparticles and quantum dots, silica particles are difficult to directly and uniformly suspend in aqueous solutions with different salinities.[108,109] Additional details on practical advantages of the present design are provided in the Supporting Information. The proposed design provides a simple model that includes fundamental features of a hybrid material based vaccine. However, for laboratory preparation of such material, amorphous silica are preferred.[110] Studying amorphous silica computationally is difficult due to the large range of surface silicate group densities that can be obtained under various conditions and the associated range of different interactions with proteins;[111] crystalline silica is more tractable for computer simulations. Our focus is on understanding the effects of factors such as atomic forces, interaction energetics, friction imposed by neighboring loops, allostery, and inertia on the structure and function of L1 assemblies, and thus, we attached our protein models to a 100-surface of crystalline silica.[79] With these factors well understood, additional complexities in hybrid vaccine design arising from the use of amorphous silica can be addressed in future work; for the purpose of this study the use of crystalline silica is a reasonable compromise. One additional design component that we found to be important is that the silica surface must be curved, ideally, resembling the surface curvature found in the VLP. Our final model design protocol is illustrated in Figure 7. First, the flat silica surface is brought in proximity to the VLP from the inside of the capsid. Then the silica atoms on the surface edge facing the interior wall of the capsid are steered toward atoms on the VLP wall. Since overall stability, geometry, and nearest-neighbor interactions within silica are maintained using harmonic restraints, steered motion of atoms on the edges of the silica sheet gradually couples to those toward the interior. Consequently, the surface buckles forming a hydrophilic convex face with radius of curvature similar to that of the interior of the $T = 1$ VLP. Next, the pentamer is tethered to the alkyl-amino groups across the surface where the silica curvature matches the inherent curvature of VLP-confined pentamer. If the silicon surface is left flat, the match of structural fluctuations between the silica-tethered pentamer and the VLP becomes less ideal, as shown in magenta color in Figure 6. In addition, there are notable, nontrivial structural consequences of the flat silica surface, on which we elaborate in the Supporting Information.

The epitope fluctuation characteristics of the pentamer covalently attached to the curved silica surface are remarkably close to that of the full VLP, as shown in Figure 6 in blue compared to the $T = 1$ VLP fluctuations shown in green.
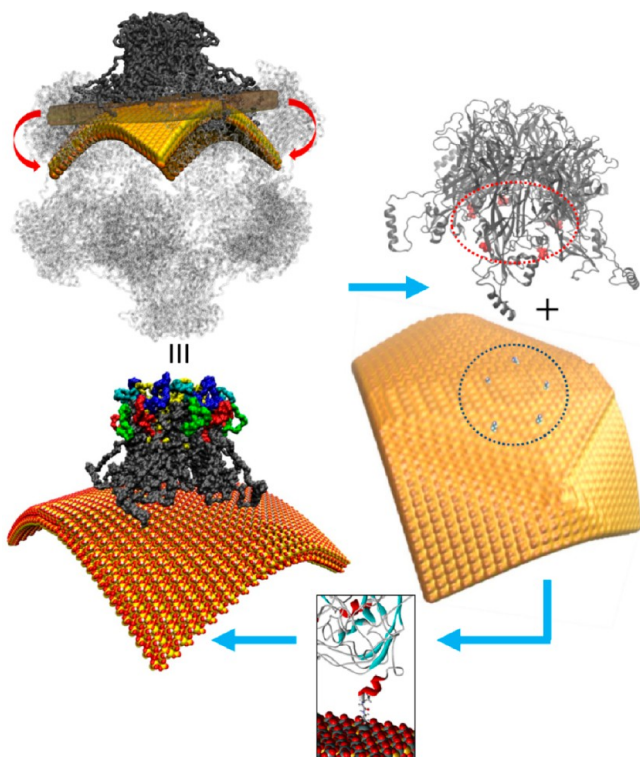
18464

dx.doi.org/10.1021/ja407489r | J. Am. Chem. Soc. 2013, 135, 18458−18468

Figure 7. Hybrid design protocol: First, a flat sheet of silica generated using CHARMM is curved using the $T = 1$ VLP as a template. Then, tethers are planted on the curved hydrophilic silica surface forming a $-Si\text{-}O\text{-}(CH_2)_3\text{-}NH_2$ linkage. Finally an L1 pentamer is attached to the surface via the tethers with the connectivity $silica-Si-O-(CH_2)_3-NH-CO-L1$.

Engineering the structural and dynamic properties of the epitope containing loops is a necessary condition for eliciting the desired immune response, but there are additional conditions that must be met to faithfully reproduce the immunogenic properties of the wild-type virus and/or the full-scale VLP. Several atomic scale features have previously been identified to be important for eliciting a proper immune response. For example, mouse monoclonal antibody H16.V5 binds to a major part of the FG loop and neutralizes HPV16;[112] mutation of ASN-285 leads to the failure of this antibody binding, suggesting that ASN-285 is directly involved in the H16.V5 binding.[112] Similarly, SER-282 appears to be important for the epitope to bind another antibody, H16.E70.[112] These

experimental observations emphasize that immune response to the L1 epitopes strongly depends on the details of the epitope structure. Fine scale structural details must therefore be carefully accounted for within a design strategy for assembling an artificial hybrid vaccine. Hydrogen bonds play a particularly important role, and we have carefully monitored the hydrogen-bond network that organizes the orientation of the epitopes to each other. Two hydrogen bonds were especially interesting: The THR-266 residue of the FG-loop forms a strong interloop hydrogen bond with an ASN-357 residue on a neighboring HI loop in the pentamer, as shown in Figure 8. This is an important structural feature also found in the VLP that must be preserved for proper immune response; it is impossible to form this interloop hydrogen-bond in a monomer, which is one of the reasons why the L1 monomer is unlikely to be useful as a vaccine. A second hydrogen bond of importance involves the residues 280−285, which enforce a relatively consistent conformation in that part of the FG loop by engaging in a network of mutually exchangeable hydrogen bonds with each other. In Figure 8 we depict one such hydrogen-bonded snapshot structure, where SER-280 and ASN-285 formed a hydrogen bond. As a consequence of these intraloop hydrogen bonds, the FG loop adopts a helix-like secondary structure, as illustrated in the detailed view of this region in Figure 8. As this portion of the FG loop is most solvent accessible, the helix-like folding provides an energetic advantage. This structural detail is present in the VLP, and we propose that it is an important recognition motif that must be preserved in a vaccine to elicit a proper immune response.[112] Note that the positional variance profiles (Figure 6) have consistently indicated a very large change in positional variance around residue 280 when moving from a monomer to higher order assemblies; this hydrogen-bond network is responsible for the significant change in the fluctuation profile, as it is not present in the monomer and the residues around 280 have a much higher degree of structural freedom. These delicate structural details support and amplify the dynamic allosteric effects of the h4 helix discussed above to ultimately generate a structural fluctuation profile of the epitopes in the silica-mounted pentamer that is essentially identical to what is seen in the much larger $T = 1$ VLP of HPV 16.

■ CONCLUSIONS

The preparation of well-defined small subassemblies, such as the pentamer, from monomeric L1 proteins is much easier[113] than synthesizing the larger assemblies like the $T = 1$ or 7
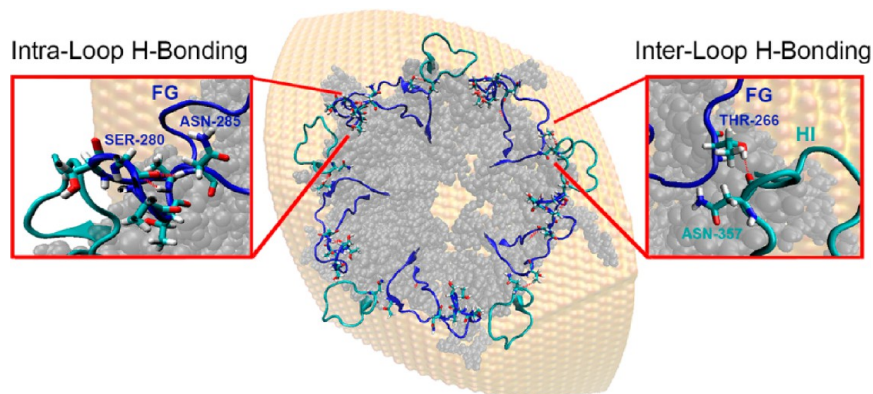

Figure 8. Organization of the surface epitopes FG and HI using inter- and intraloop hydrogen bonds.

icosahedra. Thus, the vaccine development process could be expedited significantly if the smaller particles can be used to elicit a immune response instead of having to prepare the much more elaborate VLP structures.[114] The difficulty of assembling the higher order constructs lies in the strong contribution that entropy makes to the energetics of the VLP; enthalpically, the interactions between the monomers in the pentamer assembly are much stronger than those between pentamers in the VLP. Thus, the translational entropy penalty associated with the formation of the pentamer from monomers is partially compensated for, allowing the free energy of assembly to be much more favorable for the pentamer than for the VLP.[115] Therefore, the pentamers are ideal targets in a rational vaccine design strategy. Mounting the pentamer on a silica nanoparticle is enthalpically highly favorable, i.e., the enthalpy of tether-mediated pentamer binding to silica is much higher than the interaction between pentamers to afford the VLP (Figure S8). By providing a minimally invasive chemical modification to install the chemical anchor for coupling the pentamer to the surface-modified silica nanoparticle, we introduce an additional driving force and engineer precise control over the assembly. In comparison, the preparation of the VLP from the pentamers is much more demanding, as the entropic penalties originating from the required precise relative orientation of the pentamers during the final assembly to the VLPs must be overcome.

Computer simulations have become a standard tool of biomedical research over the last few decades, but they are mainly used to rationalize and confirm experimental observations.[116−119] Given the level of sophistication and degree of realism in today's computer models, truly predictive computer modeling is not only possible but also bears significant advantages over purely experimental approaches, as we demonstrate in this work by deriving a logical and rational vaccine design strategy. To the best of our knowledge, this is the first computational study that used all-atom structures of hybrid silica-protein nanoconstructs to provide a novel nanoscale perspective on a long-standing challenge of VLP-based vaccine design. We discovered an intriguing dynamic allosteric coupling between the h4 helix and the epitope containing loops and devised an effective exploitation strategy for rigidifying the epitopes to reproduce the structural and dynamic properties of these epitopes in the VLP using the silica surface mounted pentamer. A silica mounted VLP as a basis of a vaccine against porcine virus[69] was reported previously and served as an inspiration of this work. Silica nanoparticles provide a potentially revolutionary opportunity for developing vaccines, and we demonstrate how they can be utilized rationally. Our work highlights an intriguing connection between structure, dynamics, and function, while explicitly outlining a strategy for exploiting dynamic allostery which is a relatively new concept that remains poorly understood. Our design has advantages over traditional $T = 1$ VLPs in that they are expected to be thermally stable, easy to prepare, and genome-free. Furthermore, silica nanoparticles are already FDA approved but remain an underutilized resource in vaccine development. In ongoing work, these theoretically identified vaccine candidates will be prepared and characterized in collaboration with experimentalists to test our hypothesis; whereas adjustments and improvements to our initial strategies discussed above are expected, the foundation of the control mechanisms that we identified and explained above is generally valid. In addition to the obvious benefit of having identified a specific vaccine development strategy, the dynamic allosteric control mechanism outlined in this work appears to be generally applicable and more common than previously thought and deserves further investigation.

■ ASSOCIATED CONTENT

Ⓢ Supporting Information

Computational details, additional figures, and discussion. This material is available free of charge via the Internet at http://pubs.acs.org.

■ AUTHOR INFORMATION

Corresponding Authors
mbaik@indiana.edu
ortoleva@indiana.edu

Author Contributions
[§]These authors contributed equally.

Notes
The authors declare no competing financial interest.

■ ACKNOWLEDGMENTS

■ REFERENCES

(1) Grgacic, E. V. L; Anderson, D. A. *Methods* **2006**, *40*, 60−65.
(2) Georgens, C.; Weyermann, J.; Zimmer, A. *Curr. Pharm. Biotechnol.* **2005**, *6*, 49−55.
(3) Cubas, R.; Zhang, S.; Kwon, S.; Sevick-Muraca, E. M.; Li, M.; Chen, C.; Yao, Q. *J. Immunother.* **2009**, *32*, 118−128.
(4) Jennings, G. T.; Bachmann, M. F. *Biol. Chem.* **2008**, *389*, 521−536.
(5) Ault, K. A.; Giuliano, A. R.; Edwards, R. P.; Tamms, G.; Kim, L. L.; Smith, J. F.; Jansen, K. U.; Allende, M.; Taddeo, F. J.; Skulsky, D.; Barr, E. *Vaccine* **2004**, *22*, 3004−3007.
(6) Han, J. E.; Wui, S. R.; Park, S. A.; Lee, N. G.; Kim, K. S.; Cho, Y. J.; Kim, H. J. *Vaccine* **2012**, *30*, 4127−4134.
(7) Buonaguro, L.; Tagliamonte, M.; Tornesello, M. L.; Buonaguro, F. M. *Expert Rev. Vaccines* **2011**, *10*, 1569−1583.
(8) Stanley, M.; Pinto, L. A.; Trimble, C. *Vaccine* **2012**, *30* (Suppl 5), F83−87.
(9) Foldvari, M.; Kumar, P. *Ther. Delivery* **2012**, *3*, 1005−1017.
(10) Jemon, K.; Young, V.; Wilson, M.; McKee, S.; Ward, V.; Baird, M.; Young, S.; Hibma, M. *PLoS One* **2013**, *8*, e66866.
(11) Brown, D. R.; Garland, S.; Ferris, D. G.; Joura, E.; Steben, M.; James, M.; Radley, D.; Vuocolo, S.; Garner, E. I. O.; Haupt, R. M.; Bryan, J. T. *Hum. Vaccines* **2011**, *7*, 230−238.
(12) Smith, J. F.; Brownlow, M.; Brown, M.; Kowalski, R.; Esser, M. T.; Wruiz, W.; Barr, E.; Brown, D. R.; Brian, J. T. *Hum. Vaccines* **2007**, *3*, 109−115.
(13) Chaplin, S.; Nicholas, N. *Prescriber* **2008**, *19*, 46−50.
(14) Einstein, M. H.; Baron, M.; Levin, M. J.; Chatterjee, A.; Edwards, R. P.; Zepp, F.; Carletti, I.; Dessy, F. J.; Trofa, A. F.; Schuind, A.; Dubin, G. *Hum. Vaccines* **2009**, *5*, 705−719.
(15) Metz, S. W; Gardner, J.; Geertsema, C.; Le, T. T.; Goh, L.; Vlak, J. M.; Suhrbier, A.; Gijlman, G. P. *PLoS Neglected Trop. Dis.* **2013**, *7*, e2124.
(16) Akahata, W.; Yang, Z.-Y.; Andersen, H.; Sun, S.; Holdaway, H. A.; Kong, W.-P.; Lewis, M. G.; Higgs, S.; Rossmann, M. G.; Rao, S.; Nabel, G. J. *Nat. Med.* **2010**, *16*, 334−338.

18466

dx.doi.org/10.1021/ja407489r | *J. Am. Chem. Soc.* 2013, 135, 18458−18468

(17) Guu, T. S. Y.; Liu, Z.; Ye, Q.; Mata, D. A.; Li, K.; Yin, C.; Zhang, J.; Tao, Y. J. *Proc. Natl. Acad. Sci. U.S.A.* **2009**, *106*, 12992−12997.

(18) Li, T.-C.; Suzaki, Y.; Ami, Y.; Dhole, T. N.; Miyamura, T.; Takeda, N. *Vaccine* **2004**, *22*, 370−377.

(19) Jennings, G. T.; Bachmann, M. F. *Annu. Rev. Pharmacol. Toxicol.* **2009**, *49*, 303−326.

(20) Roldão, A.; Mellado, M. C. M.; Castilho, L. R.; Carrondo, M. J. T.; Alves, P. M. *Expert Rev. Vaccines* **2010**, *9*, 1149−1176.

(21) Da Silva, D. M.; Schiller, J. T.; Kast, W. M. *Vaccine* **2003**, *21*, 3219−3227.

(22) Pushko, P.; Pumpens, P.; Grens, E. *Intervirology* **2013**, *56*, 141−165.

(23) Lehtinen, M.; Dillner, J. *Nat. Rev. Clin. Oncol.* **2013**, *10*, 400−410.

(24) Loucq, C. *Clin Exp Vaccine Res.* **2013**, *2*, 4−7.

(25) Bárcena, J.; Blanco, E. *Subcell. Biochem.* **2013**, *68*, 631−665.

(26) Brown, D. R.; Kjaer, S. K.; Sigurdsson, K.; Iverson, O.-E.; Hernandez-Avila, M.; Wheeler, C. M.; Perez, G.; Koutsky, L. A.; Tay, E. H.; Garcia, P.; Ault, K. A.; Garland, S. M.; Leodolter, S.; Olsson, S.-E.; Tang, G. W. K.; Ferris, D. G.; Paavonen, J.; Steben, M.; Bosch, F. X.; Dillner, J.; Joura, E. A.; Kurman, R. J.; Majewski, S.; Muñoz, N.; Myers, E. R.; Villa, L. L.; Taddeo, F. J.; Roberts, C.; Tadesse, A.; Bryan, J.; Lupinacci, L. C.; Giacoletti, K. E. D.; Sings, H. L.; James, M.; Hesley, T. M.; Barr, E. *J. Infect. Dis.* **2009**, *199*, 926−935.

(27) Dillner, J.; Kjaer, S. K.; Wheeler, C. M.; Sigurdsson, K.; Iversen, O. E.; Hernandez-Avila, M.; Perez, G.; Brown, D. R.; Koutsky, L. A.; Tay, E. H.; Garcia, P.; Ault, K. A.; Garland, S. M.; Leodolter, S.; Olsson, S. E.; Tang, G. W.; Ferris, D. G.; Paavonen, J.; Lehtinen, M.; Steben, M.; Bosch, F. X.; Joura, E. A.; Majewski, S.; Munoz, N.; Myers, E. R.; Villa, L. L.; Taddeo, F. J.; Roberts, C.; Tadesse, A.; Bryan, J. T.; Maansson, R.; Lu, S.; Vuocolo, S.; Hesley, T. M.; Barr, E.; Haupt, R. *Br. Med. J.* **2010**, *341*, c3493.

(28) The FUTURE II Study Group. *New Eng. J. Med.* **2007**, *356*, 1915−1927.

(29) Wheeler, C. M.; et al. *J. Infect. Dis.* **2009**, *199*, 936−944.

(30) Tota, J. E.; Ramanakumar, A. V.; Jiang, M.; Dillner, J.; Walter, S. D.; Kaufman, J. S.; Coutlée, F.; Villa, L. L.; Franco, E. L. *Am. J. Epidemiol.* **2013**, *178*, 625−634.

(31) de Villiers, E.-M.; Fauquet, C.; Broker, T. R.; Bernard, H.-U.; zur Hausen, H. *Virology* **2004**, *324*, 17−27.

(32) Schulz, R.; Lindner, B.; Petridis, L.; Smith, J. C. *J. Chem. Theory Comput.* **2009**, *5*, 2798−2808.

(33) Sanbonmatsu, K. Y.; Tung, C. S. *J. Struct. Biol.* **2007**, *157*, 470−480.

(34) Nakano, A.; Kalia, R. K.; Nomura, K.; Sharma, A.; Vashista, P.; Shimojo, F.; van Duin, A. C. T.; Goddard, W. A.; Biswas, R.; Srivastava, D.; Yang, L. H. *Int. J. High Perf. Comput. Applic.* **2008**, *22*, 113−128.

(35) Saunders, M. G.; Voth, G. A. *Curr. Opin. Struct. Biol.* **2012**, *22*, 144−150.

(36) Joshi, H.; Singharoy, A. B.; Sereda, Y. V.; Cheluvaraja, S. C.; Ortoleva, P. J. *Progr. Biophys. Mol. Biol.* **2011**, *107*, 200−217.

(37) Miao, Y.; Johnson, J. E.; Ortoleva, P. J. *J. Phys. Chem. B* **2010**, *114*, 11181−11195.

(38) Freddolino, P. L.; Arkhipov, A. S.; Larson, S. B.; McPherson, A.; Schulten, K. *Structure* **2006**, *14*, 437−449.

(39) Ode, H.; Nakashima, M.; Kitamura, S.; Sugiura, W.; H, S. *Front. Microbiol.* **2012**, *3*, 258.

(40) Joshi, H.; Cheluvaraja, S.; Somogyi, E.; Brown, D. R.; Ortoleva, P. J. *Vaccine* **2011**, *29*, 9423−9430.

(41) Bishop, B.; Dasgupta, J.; Klein, M.; Garcea, R. L.; Christensen, N. D.; Zhao, R. *J. Biol. Chem.* **2007**, *282*, 31803−31811.

(42) Chen, X. S.; Garcea, R. L.; Goldberg, I.; Casini, G.; Harrison, S. C. *Mol. Cell* **2000**, *5*, 557−567.

(43) Bishop, B.; Dasgupta, J.; Chen, X. *Virol. J.* **2007**, *4*, 3.

(44) Ryding, J.; Dahlberg, L.; Wallen-Ohmann, M.; Dillner, J. *J. Gen. Vir.* **2007**, *88*, 792−802.

(45) Roden, R.; Armstrong, A.; Haderer, P.; Christensen, N.; Hubbert, N.; Lowy, D.; Schiller, J.; Kirnbauer, R. *J. Virol.* **1997**, *71*, 6247−6252.

(46) Nowak, M. A. *Sem. Virol.* **1996**, *7*, 83−92.

(47) Stanley, M.; Lowy, D. R.; Frazer, I. *Vaccine* **2006**, *24* (Supplement 3), S106−S113.

(48) Christensen, N. D.; Cladel, N. M.; Reed, C. A.; Budgeon, L. R.; Embers, M. E.; Skulsky, D. M.; McClements, W. L.; Ludmerer, S. W.; Jansen, K. U. *Virology* **2001**, *291*, 324−334.

(49) Carter, J. J.; Wipf, G. C.; Madeleine, M. M.; Schwartz, S. M.; Koutsky, L. A.; Galloway, D. A. *J. Virol.* **2006**, *80*, 4664−4672.

(50) Thönes, N.; Müller, M. *Virology* **2007**, *369*, 375−388.

(51) Schädlich, L.; Senger, T.; Gerlach, B.; Mücke, N.; Klein, C.; Bravo, I. G.; Müller, M.; Gissmann, L. *J. Virol.* **2009**, *83*, 7690−7705.

(52) Zhao, Q.; Allen, M. J.; Wang, Y.; Wang, B.; Wang, N.; Shi, L.; Sitrin, R. D. *J. Nanomed. Nanotechnol.* **2012**, *8*, 1182−1189.

(53) Giedroc, D. P.; Arunkumar, A. I. *Dalton Trans.* **2007**, 3107−3120.

(54) Monod, J.; Changeux, J. P.; Jacob, F. *J. Mol. Biol.* **1963**, *6*, 306.

(55) Monod, J.; Wyman, J.; Changeux, J. P. *J. Mol. Biol.* **1965**, *12*, 88.

(56) Tzeng, S.-R.; Kalodimos, C. G. *Nature* **2009**, *462*, 368−372.

(57) Weinkam, P.; Pons, J.; Sali, A. *Proc. Natl. Acad. Sci. U.S.A.* **2012**, *109*, 4875−4880.

(58) Kalodimos, C. G.; Nyas. *Ann. N.Y. Acad. Sci.* **2012**, *1260*, 81−86.

(59) Kern, D.; Zuiderweg, E. R. P. *Curr. Opin. Struct. Biol.* **2003**, *13*, 748−757.

(60) Brunori, M. *Protein Sci.* **2011**, *20*, 1097−1099.

(61) Changeux, J. P.; Edelstein, S. J. *Science* **2005**, *308*, 1424−1428.

(62) Freire, E. *Proc. Natl. Acad. Sci. U.S.A.* **2000**, *97*, 11680−11682.

(63) Hilser, V. J. *Science* **2010**, *327*, 653−654.

(64) Tsai, C. J.; del Sol, A.; Nussinov, R. *J. Mol. Biol.* **2008**, *378*, 1−11.

(65) Daily, M. D.; Gray, J. J. *Proteins* **2007**, *67*, 385−399.

(66) Swain, J. F.; Gierasch, L. M. *Curr. Opin. Struct. Biol.* **2006**, *16*, 102−108.

(67) Gunasekaran, K.; Ma, B. Y.; Nussinov, R. *Proteins* **2004**, *57*, 433−443.

(68) Hawkins, R. J.; McLeish, T. C. B. *J. R. Soc., Interface* **2006**, *3*, 125−138.

(69) Guo, H. C.; Feng, X. M.; Sun, S. Q.; Wei, Y. Q.; Sun, D. H.; Liu, X. T.; Liu, Z. X.; Luo, J. X.; Hong, Y. *Virol. J.* **2012**, *9*, 108.

(70) Benezra, M.; Penate-Medina, O.; Zanzonico, P. B.; Schaer, D.; Ow, H.; Burns, A.; DeStanchina, E.; Longo, V.; Herz, E.; Iyer, S.; Wolchok, J.; Larson, S. M.; Wiesner, U.; Bradbury, M. S. *J. Clin. Invest.* **2011**, *121*, 2768−2780.

(71) Kumar, S.; Huang, C.; Zheng, G.; Bohm, E.; Bhatele, A.; Phillips, J. C.; Yu, H.; Kale, L. V. *IBM J. Res. Dev.* **2008**, *52*, 177−188.

(72) Phillips, J. C.; Braun, R.; Wang, W.; Gumbart, J.; Tajkhorshid, E.; Villa, E.; Chipot, C.; Skeel, R. D.; Kale, L.; Schulten, K. *J. Comput. Chem.* **2005**, *26*, 1781−1802.

(73) Carrillo-Tripp, M.; Shepherd, C. M.; Borelli, I. A.; Venkataraman, S.; Lander, G.; Natarajan, P.; Johnson, J. E.; Brooks, C. L., III; Reddy, V. S. *Nucleic Acids Res.* **2009**, *37*, D436−D442.

(74) Jorgensen, W. L.; Chandrasekhar, J.; Madura, J. D.; Impey, R. W.; Klein, M. L. *J. Chem. Phys.* **1983**, *79*, 926−935.

(75) Humphrey, W.; Dalke, A.; Schulten, K. *J. Mol. Graphics* **1996**, *14*, 33−38.

(76) Brooks, B. R.; Brooks, C. L., III; Mackerell, A. D.; Nilsson, L.; Petrella, R. J.; Roux, B.; Won, Y.; Archontis, G.; Bartels, C.; A., B.; Caflisch, S.; Caves, L.; Cui, Q.; Dinner, A. R.; Feig, M.; Fischer, S.; Gao, J.; Hodoscek, M.; Im, W.; Kuczera, K.; Lazaridis, T.; Ma, J.; Ovchinnikov, V.; Paci, E.; Pastor, R. W.; Post, C. B.; Pu, J. Z.; Schaefer, M.; Tidor, B.; Venable, R. M.; Woodcock, H. L.; Wu, X.; Yang, W.; York, D. M.; Karplus, M. *J. Comput. Chem.* **2009**, *30*, 1545−1614.

(77) MacKerell, A. D.; Banavali, N.; Foloppe, N. *Biopolymers* **2000**, *56*, 257−265.

(78) Foloppe, N.; MacKerell, A. D. *J. Comput. Chem.* **2000**, *21*, 86−104.

(79) Lopes, P. E. M.; Murashov, V.; Tazi, M.; Demchuk, E.; MacKerell, A. D. *J. Phys. Chem. B* **2006**, *110*, 2782−2792.

(80) *Jaguar 7.0*; Schrödinger, Inc.: New York, 2013.

(81) Myung, S.; Lorton, K. P.; Merenbloom, S. I.; Fioroni, M.; Koeniger, S. L.; Julian, R. R.; Baik, M.-H.; Clemmer, D. E. *J. Am. Chem. Soc.* **2006**, *128*, 15988−15989.

(82) Mantri, Y.; Fioroni, M.; Baik, M.-H. *J. Biol. Inorg. Chem.* **2008**, *13*, 1197−1204.

(83) The loops BC and DE exhibit very similar structural and dynamic properties as the other three loops we discuss explicitly. Thus, although we do not discuss the property changes of BC and DE loops specifically in the main text, our main conclusions are not impacted by this omission.

(84) Details are given in the Supporting Information.

(85) Note that the loops BC and DE are not marked, but they are also strongly correlated.

(86) See Supporting Information for additional discussions.

(87) Grossoehme, N. E.; Giedroc, D. P. *Methods Mol. Biol.* **2012**, *796*, 31−51.

(88) Guerra, A. J.; Giedroc, D. P. *Arch. Biochem. Biophys.* **2012**, *519*, 210−222.

(89) Reyes-Caballero, H.; Campanello, G. C.; Giedroc, D. P. *Biophys. Chem.* **2011**, *156*, 103−114.

(90) Cooper, A.; Dryden, D. T. F. *Eur. Biophys. J. Biophy.* **1984**, *11*, 103−109.

(91) del Sol, A.; Tsai, C. J.; Ma, B. Y.; Nussinov, R. *Structure* **2009**, *17*, 1042−1050.

(92) Tsai, C. J.; Del Sol, A.; Nussinov, R. *Mol. Biosyst.* **2009**, *5*, 207−216.

(93) Hawkins, R. J.; McLeish, T. C. B., *Phys. Rev. Lett.* **2004**, *93*.

(94) Long, D.; Bruschweiler, R. *J. Phys. Chem. Lett.* **2012**, *3*, 1722−1726.

(95) Tsai, C.-J.; del Sol, A.; Nussinov, R. *J. Mol. Biol.* **2008**, *378*, 1−11.

(96) Hawkins, R. J.; McLeish, T. C. B. *Biophys. J.* **2006**, *91*, 2055−2062.

(97) Rohs, R.; Bloch, I.; Sklenar, H.; Shakked, Z. *Nucleic Acids Res.* **2005**, *33*, 7048−7057.

(98) Joshi, H.; Lewis, K.; Singharoy, A.; Ortoleva, P. J. *Vaccine* **2013**, *31*, 4841−4847.

(99) Vertegel, A. A.; Siegel, R. W.; Dordick, J. S. *Langmuir* **2004**, *20*, 6800−6807.

(100) Sun; al., e. *Proc. Natl. Acad. Sci. U.S.A* **2007**, *104*, 1354−1359.

(101) Meyers, M. A.; Chen, P.-Y.; Lin, A. Y.-M.; Seki, Y. *Progr. Mater. Sci.* **2008**, *53*, 1−206.

(102) Kneuer, C.; Sameti, M.; Haltner, E. G.; Schiestel, T.; Schirra, H.; Schmidt, H.; Lehr, C.-M. *Int. J. Pharm.* **2000**, *196*, 257−261.

(103) Parida, S. K.; Dash, S.; Patel, S.; Mishra, B. *Adv. Colloid Interfac.* **2006**, *121*, 77−110.

(104) Pattabiraman, V. R.; Bode, J. W. *Nature* **2011**, *480*, 471−479.

(105) Li, X.; Yang, T.; Gao, Q.; Yuan, J.; Cheng, S. *J. Colloid Interface Sci.* **2009**, *338*, 99−104.

(106) Knopp, D.; Tang, D.; Niessner, R. *Anal. Chim. Acta* **2009**, *647*, 14−30.

(107) Barandeh, F.; Nguyen, P-L; Kumar, R.; Iacobucci, G. J.; Kuznicki, M. L.; Kosterman, Andrew; Bergey, Earl J.; Prasad, Paras N.; Gunawardena, S. *PLoS One* **2012**, *7*, e29424.

(108) Aubin-Tam, M. E.; Hamad-Schifferli, K. *Biomed. Mater.* **2008**, *3*, 034001.

(109) Sperling, R. A.; Parak, W. J. *Philos. Trans. R. Soc., A* **2010**, *368*, 1333−1383.

(110) Jin, Y.; Li, A.; Hazelton, S. G.; Liang, S.; John, C. L.; Selid, P. D.; Pierce, D. T.; Zhao, J. X. *Coord. Chem. Rev.* **2009**, *253*, 2998−3014.

(111) Cruz-Chu, E. R.; Aksimentiev, A.; Schulten, K. *J. Phys. Chem. B* **2006**, *110*, 21497−21508.

(112) White, W. I.; Wilson, S. D.; Palmer-Hill, F. J.; Woods, R. M.; Ghim, S.-j.; Hewitt, L. A.; Goldman, D. M.; Burke, S. J.; Jenson, A. B.; Koenig, S.; Suzich, J. A. *J. Virol.* **1999**, *73*, 4882−4889.

(113) Thönes, N.; Herreiner, A.; Schädlich, L.; Piuko, K.; Müller, M. *J. Virol.* **2008**, *82*, 5472−5485.

(114) Zlotnick, A. *J. Mol. Recognit.* **2005**, *18*, 479−490.

(115) Quick, R.; Singharoy, A.; Ortoleva, P. *Chem. Phys. Lett.* **2013**, *571*, 61−65.

(116) Takada, S. *Curr. Opin. Struct. Biol.* **2012**, *22*, 130−137.

(117) Durrant, J.; McCammon, J. *BMC Biol.* **2011**, *9*, 71.

(118) Cheatham, T. E., III; Kollman, P. A. *Annu. Rev. Phys. Chem.* **2000**, *51*, 435−471.

(119) Karplus, M.; McCammon, J. A. *Nat. Struct. Mol. Biol.* **2002**, *9*, 646−652.

(120) Tang, F.; Li, L.; Chen, D. *Adv. Mater.* **2012**, *24*, 1504−1534.